Acta Oceanol. Sin., 2024, Vol. 43, No. 6, P. 163–172
https://doi.org/10.1007/s13131-024-2309-8
http://www.aosocean.com
E-mail: ocean2@hyxb.org.cn

Effects of nutrient limitations on the sinking velocity of *Thalassiosira weissflogii*

Jie Zhu[1, 2, 3], Qiang Hao[2, 3], Wei Zhang[2, 3, 4], Yingying Ma[5], Jiangning Zeng[1, 2, 3, 4*]

[1] Ocean College, Zhejiang University, Zhoushan 316000, China

[2] Second Institute of Oceanography, Ministry of Natural Resources, Hangzhou 310012, China

[3] Key Laboratory of Marine Ecosystem Dynamics, Ministry of Natural Resources, Hangzhou 310012, China

[4] Zhejiang Key Laboratory of Nearshore Engineering Environment and Ecological Security, Hangzhou 310012, China

[5] Tianjin Key Lab of Aqua-Ecology and Aquaculture, College of Fisheries, Tianjin Agricultural University, Tianjin 300384, China

Received 17 September 2023; accepted 15 January 2024

Abstract

The sinking of diatoms is critical to the formation of oceanic biological pumps and coastal hypoxic zones. However, little is known about the effects of different nutrient restrictions on diatom sinking. In this study, we measured the sinking velocity (SV) of *Thalassiosira weissflogii* using a new phytoplankton video observation instrument and analyzed major biochemical components under varying nutrient conditions. Our results showed that the SV of *T. weissflogii* under different nutrient limitation conditions varied substantially. The highest SV of (1.77 ± 0.02) m/d was obtained under nitrate limitation, significantly surpassing that under phosphate limitation at (0.98 ± 0.13) m/d. As the nutrient limitation was released, the SV steadily decreased to (0.32 ± 0.03) m/d and (0.15 ± 0.05) m/d, respectively. Notably, under conditions with limited nitrate and phosphate concentrations, the SV values of *T. weissflogii* significantly positively correlated with the lipid content ($P < 0.001$), with R^2 values of 0.86 and 0.69, respectively. The change of the phytoplankton SV was primarily related to the intracellular composition, which is controlled by nutrient conditions but did not significantly correlate with transparent extracellular polymer and biosilica contents. The results of this study help to understand the regulation of the vertical sinking process of diatoms by nutrient restriction and provide new insights into phytoplankton dynamics and their relationship with the marine nutrient structure.

Key words: nutrient limitation, *Thalassiosira weissflogii*, sinking velocity, biochemical component, lipid content

Citation: Zhu Jie, Hao Qiang, Zhang Wei, Ma Yingying, Zeng Jiangning. 2024. Effects of nutrient limitations on the sinking velocity of *Thalassiosira weissflogii*. Acta Oceanologica Sinica, 43(6): 163–172, doi: 10.1007/s13131-024-2309-8

1 Introduction

Nutrients are one of the key factors regulating marine phytoplankton dynamics. Recently, nutrient pollution in China's offshore waters has become more serious. The excessive input of nitrate and phosphate nutrients has led to an imbalance in the nitrogen–phosphorus ratio, in turn triggering ecological disaster phenomena such as large-scale harmful algal blooms, hypoxia, and eutrophication (Li et al., 2002; Tang et al., 2006; Yu et al., 2018; Wang et al., 2022). These phenomena seriously threaten both phytoplankton growth and the overall health of aquatic ecosystems. As the main phytoplankton group in the offshore waters of China, diatoms play an important role in the global ocean carbon cycle and biogeochemistry and strongly correlate with the formation of summer hypoxic conditions (Cloern, 2001; Turner et al., 2006; Conle et al., 2009; Wang et al., 2017). Physiological conditions and migratory changes of diatoms exert substantial effects on the stability of marine ecosystems (Jin et al., 2006; Tréguer et al., 2018; Zhou et al., 2020).

Sinking is an important determinant that affects the spatial distribution of phytoplankton communities and the access of individual phytoplankton cells to light and nutrient salts (Smayda, 1970; Margalef, 1978). The effects of the vertical transport of phytoplankton vary significantly (Titman and Kilham, 1976; Huisman and Sommeijer, 2002; Ptacnik et al., 2003; Durante et al., 2019). Their physiological state undeniably affects phytoplankton's sinking velocity (SV). Currently, the mechanisms that have been proposed to regulate buoyancy are primarily based on changes in the cell density, such as the selective uptake of ions (Anderson and Sweeney, 1978), production of organic osmolytes (Boyd and Gradmann, 2002), vesicle regulation (Raven and Doblin, 2014), ballast effects of carbohydrates (Lavoie et al., 2016), lipid accumulation (Anderson and Sweeney, 1977), and cyclic cell expansion (Lavoie and Raven, 2020). In addition, changes in environmental conditions, such as temperature, salinity (Bienfang and Szyper, 1982), and irradiance (Granata, 1991), as well as the reproductive state of the cells and exposure history of nutri-

Foundation item: The Key R&D Program of Zhejiang under contract No. 2023C03120; the Science Foundation of Donghai Laboratory under contract No. DH-2022KF0215; the National Key Research and Development Program of China under contract No. 2021YFC3101702; the National Programme on Global Change and Air-Sea Interaction (Phase Ⅱ)—Hypoxia and Acidification Monitoring Warning Project in the Changjiang Estuary, and Long-term Observation and Research Plan in the Changjiang Estuary and Adjacent East China Sea (LORCE) Project under contract No. SZ2001.
*Corresponding author, E-mail: jiangningz@126.com

ent concentrations (Waite and Harrison, 1992), can affect phytoplankton settling rates. Some studies have also reported that porosity is important for particle settling (Alldredge and Gotschalk, 1988; Bach et al., 2016). However, the biochemical mechanisms responsible for buoyancy regulation remain unclear, necessitating further research to unveil the specific mechanisms governing the phytoplankton sinking behavior.

The Changjiang (Yangtze) River Estuary and its adjacent waters form a globally important high-productivity shelf-edge seas and are a key area for marine phytoplankton research in China (Zhou et al., 2008). Due to the terrestrial input of high nitrate and low phosphate, the spatiotemporal changes of the nutrient structure are extremely complex, significantly influencing the ecological effect of the phytoplankton community. Based on surveys, phytoplankton growth in near-estuarine waters of the Changjiang River Estuary, is primarily limited by phosphate, whereas it may be limited by nitrate in areas far from the estuary (Wang et al., 2003; Chen et al., 2012; Liu et al., 2016). As a typical planktonic diatom with high silicification and strong survival ability, *Thalassiosira weissflogii* is a common dominant algal species in the waters of the Changjiang River Estuary, which has an important ecological status and good research value (d'Ippolito et al., 2015; Botte et al., 2018).

In this study, we focused on *T. weissflogii*, simulated the nutrient-limited environment of the Changjiang River Estuary, and explored the effects of nutrient repletion, nutrient limitation, and nutrient depletion on *T. weissflogii* using semi-continuous and one-time culture models. Moreover, we observed the changes in sinking behavior under nutrient depletion and spiking conditions, examining the relationship between the SV and cell content (closely related to cell density, e.g., carbohydrates, proteins, lipids), as well as between biosilica and transparent extracellular polymeric particles (TEP) to analyze the buoyancy regulation mechanism of *T. weissflogii* under different nutrient limitation conditions. Our findings will provide further insights into the effect of the nutrient structure of China's coastal waters on the settlement of diatoms.

2 Materials and methods

2.1 *Diatom cultures*

The purified culture of *T. weissflogii* was used in the laboratory, based on the f/2 culture in sterile natural seawater (Guillard and Ryther, 1962), with a temperature control of 19℃, light intensity of 25 μmol photons per square meter per second and light-dark ratio of 12 h:12 h.

2.2 *Cultivation methods and experimental setup*

We aimed to investigate the effects of nutrient limitation (PO_4^{3-} and NO_3^-) on the SV of *T. weissflogii*. Based on the actual conditions of the Changjiang River Estuary and according to the Redfield ratio (N:P = 16:1), we set the experimental N:P ratio at 4:1 and 64:1 to ensure that *T. weissflogii* is absolutely limited by nutrients.

To adapt the cells to the experimental conditions, the semi-continuous culture was carried out three days before the start of each experiment using sterile natural seawater to maintain a constant biomass of algal cells. Subsequently, *T. weissflogii* in the exponential growth phase was inoculated in the sterilized f/2 medium prepared by natural seawater. The initial inoculation density was 10^4 cells/mL, the culture volume was 15 L, and the culture container was a 20 L glass bottle. Three replicates were performed for each experiment.

In the nitrate limitation experiments, the initial concentrations of nitrate and phosphate were 96 μmol/L and 24 μmol/L (N:P = 4:1), respectively. In the phosphate limitation experiments, the initial concentrations of nitrate and phosphate were 384 μmol/L and 6 μmol/L (N:P = 64:1), respectively. Silicate, trace metal elements, and vitamins were added according to the f/2 medium. During the experiments, the concentrations of non-limiting nutrients, trace metals, and vitamins were maintained to ensure that only one nutrient was limited. The strain was cultured under a light intensity of 70 μmol photon per square meter per second, with a 12 h:12 h light-dark cycle at 25℃. The culture had a salinity of 28, pH of 8.0 and was continuously stirred at 180 r/min. In the experiment, we determined the nutrient status based on the growth rate of the cells: (1) nutrient repletion (NR), log-phase growth; (2) nutrient limitation (NL), the growth rate of 0.1–0.3 d^{-1}; (3) nutrient depletion (ND), where the growth rate approaches zero. When the cell growth rate was near zero, the missing nutrient was added to the culture according to the f/2 medium concentration to induce repletion conditions in the media. This process is referred to as a nutrient spike (NS). The SV values were recorded at different nutrient stages and five-time points: NR, NL, ND, NS, and 2 h, 6 h, 12 h, 24 h, and 48 h after adding the limiting nutrient. PR, PL, PD, and PS represent phosphate repletion, phosphate limitation, phosphate depletion, and phosphate spike, respectively.

2.3 *Analysis of cell physiological status*

The cell abundance was monitored using an automated cell counter (Shanghai RuiYu Biotech Co., Ltd., China). The growth rate (μ, d^{-1}) was calculated daily as follows:

$$\mu = \frac{\ln(C_1/C_0)}{t_1 - t_0}, \tag{1}$$

where C_0 and C_1 are the cell concentrations at t_0 and t_1, respectively.

The optimal photochemical efficiency of photosystem Ⅱ (PSⅡ) was measured daily using water pulse amplitude-modulated fluorometry (Heinz Walz GmbH, 91090 Effeltrich, Germany). Samples were treated in the dark for 20 min before measuring the maximum fluorescence (F_m) and minimum fluorescence (F_0). The maximum photosynthetic quenching capacity (F_v) was calculated as the difference between F_m and F_0.

For chlorophyll *a* (Chl-*a*) analysis, the samples were filtered through 25 mm GF/F filters (pore size = 0.65 μm) under low vacuum pressure (<0.04 MPa) and stored at –20℃ in the dark. After extraction with 90% acetone for 24 h at –20℃ in the dark, Chl-*a* was measured with a Turner Designs Trilogy™ fluorometer (Caspers, 1970).

The surface area of a single cell was calculated using the electron microscope's photography and measurement function. The average cell surface area was calculated from the average cell height and average square radius under the assumption that all cells were cylinders. The number of cells observed at each stage was 30.

2.4 *Nutrient analysis*

Water samples were filtered through a polycarbonate membrane (0.45 μm) for nutrient analyses. Nutrients, such as nitrate, phosphate, and silicate, were analyzed with thymol spectrophotometry (Osibanjo and Ajayi, 1980), the molybdenum blue meth-

od (Holman, 1943), and silicon molybdenum blue method (Luke, 1953), respectively.

2.5 *Analysis of cellular biochemical fractions*

Intracellular glucose-based carbohydrates were determined using the anthrone colorimetric method (Laurentin and Edwards, 2003). Protein quantification was carried out using the Coomassie brilliant blue method (Bradford, 1976), and lipid extraction and quantification followed the protocol by Johnson and Wen (2009). Pretreatment of the algal solution was required before analyzing the glucose-based carbohydrate, protein, and lipid contents. Firstly, 1 L of culture solution was filtered through a polycarbonate membrane with a pore size of 2 μm at a vacuum pump pressure ⩽0.4 kPa and rinsed three times with distilled water. The cells were vacuum freeze-dried at –70℃ for 24 h and broken by repeated freeze-thawing cycles. The cells were frozen at a temperature below –20℃ and then thawn at ~4℃. This process was repeated 3–4 times. The formation of intracellular ice particles and increased cytoplasmic salt concentration caused the cell structure's cleavage and fragmentation.

2.6 *Transparent extracellular polymer and biosilica analysis*

The TEP concentrations (μg/L) (Xeq) were measured using a previously reported method (Passow and Alldredge, 1995) with minor modifications. Three 10 mL samples were filtered through a polycarbonate filter with a pore size of 0.4 μm under a low constant vacuum (<0.02 MPa) and stained with 0.5 mL of 0.02% Alisin Blue solution for 2 s. The filters were subsequently rinsed twice with 2 mL of distilled water to remove excess dye from the filter surface. Extraction was performed with 6 mL of 80% sulfuric acid for 2 h. The absorbance of TEP was determined at 787 nm using a spectrophotometer with xanthan gum as the base. Biosilica was quantitatively determined with chemical extraction and silicomolybdic blue spectrophotometric methods (Luke, 1953).

2.7 *SV analysis*

The SV of the cells was determined with a high-definition microscopic video system developed in the laboratory. The system was modified from that described by O'Brien et al. (2006) and consisted of a feed pump, magnetic stirrer, observation vessel, light source, and high-speed camera system. Diatoms sink slowly and are sensitive to the ambient water velocity. To minimize convection in the observation vessel, a saline gradient seawater was prepared using the method described by O'Brien et al. (2006), with the salinities set at 28 and 32 to ensure that the value in the vessel was gradually increased from the top to the bottom, thus inhibiting convection. *Thalassiosira weissflogii* cells were processed by filming in a 10 cm × 8 cm × 2 cm (width × height × depth) glass observation cell using a Light Emitting Diode infrared illumination light source. The videos were recorded at 30 frames per second for 10–20 min, allowing many individual sinking cells to be recorded and tracked. All focal cells in the video were tracked, and data were analyzed using the Image J software package TrackMate (Tinevez et al., 2017). The number of cells processed exceeded 200 at a time to ensure that the data were statistically significant.

2.8 *Data analysis*

Pearson's coefficient correlation analyses of SV and each tested parameter (F_v/F_m, growth rate, carbohydrates, proteins, lipids, biosilica, and TEP) were performed using SPSS 25.0 software. Graphing was conducted using GraphPad Prism 9.0 and R language software (4.3.0).

Before the nutrient limitation experiments, *T. weissflogii* was acclimatized to the initial nutrients for 2 d. The initial cell abundance for the two sets of experiments was 2.40 × 10^4 cells/mL and 2.10 × 10^4 cells/mL.

3 Results

Before the nutrient limitation experiments, *T. weissflogii* was acclimatized to the initial nutrients for 2 d. The initial cell abundance for the two sets of experiments was 2.40 × 10^4 cells/mL and 2.10 × 10^4 cells/mL. The cell abundance and growth rate data for the two sets of experiments are shown in Fig. 1. The maximum photochemical efficiencies (F_v/F_m) for Chl-*a* and photosystem II are shown in Fig. 2. Data on the limited nutrient concentration and sinking rates are shown in Fig. 3. Cellular contents (proteins, carbohydrates, and lipids) and TEP and BSi data are shown in Figs 4, 5, and 6, respectively. Table 1 demonstrates the status of the main parameters at different stages of the two nutrient salt limitations. The physiological and biochemical responses of

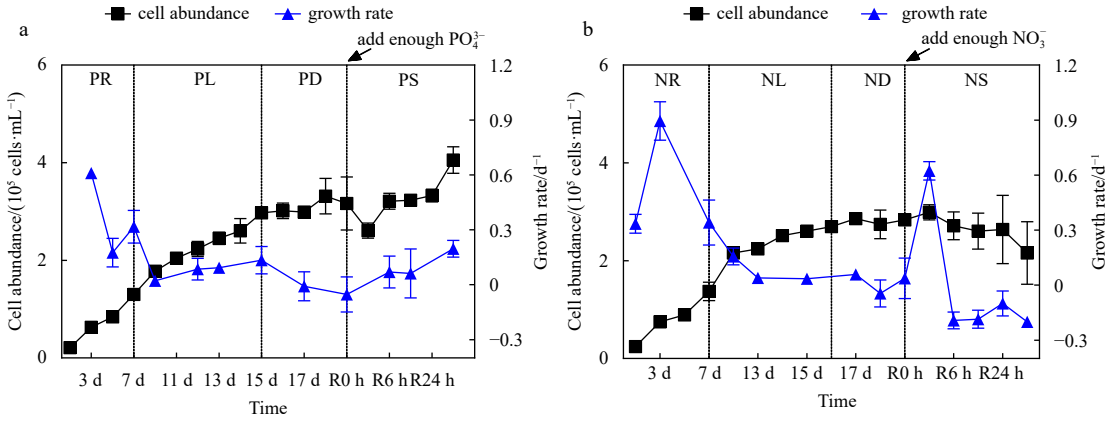

Fig. 1. Cell abundance and growth rate data for the phosphate depletion-spike experiment (a) and nitrate depletion-spike experiment (b). PR, PL, PD, and PS represent phosphate repletion, phosphate limitation, phosphate depletion, and phosphate spike, respectively. NR, NL, ND, and NS represent nitrate repletion, nitrate limitation, nitrate depletion, and nitrate spike, respectively. R represents the post-recovery time, and five-time points 2 h, 6 h, 12 h, 24 h, and 48 h were recorded after the addition of limiting nutrients. These abbreviations apply to all figures.

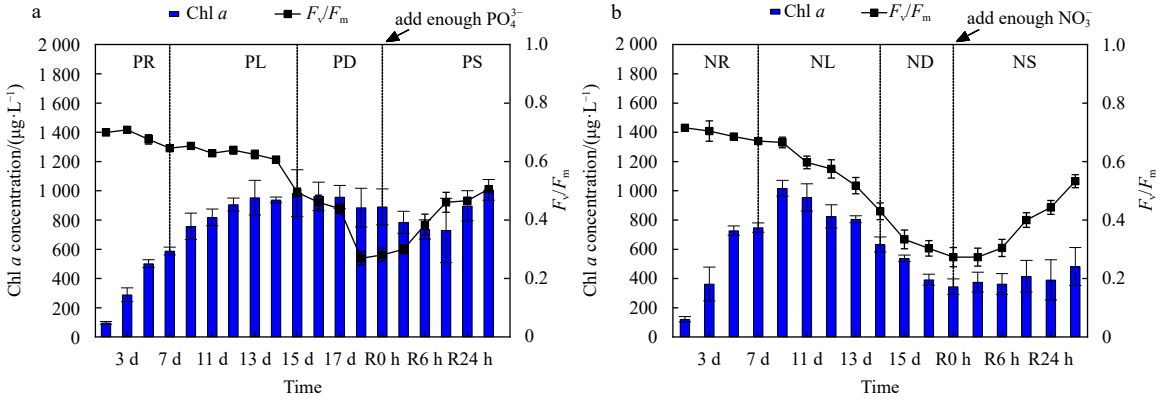

Fig. 2. Chlorophyll *a* concentrations and the changes in the optimal photochemical efficiency of photosystem Ⅱ (F_v/F_m) throughout the phosphate depletion-spike experiment (a) and nitrate depletion-spike experiment (b).

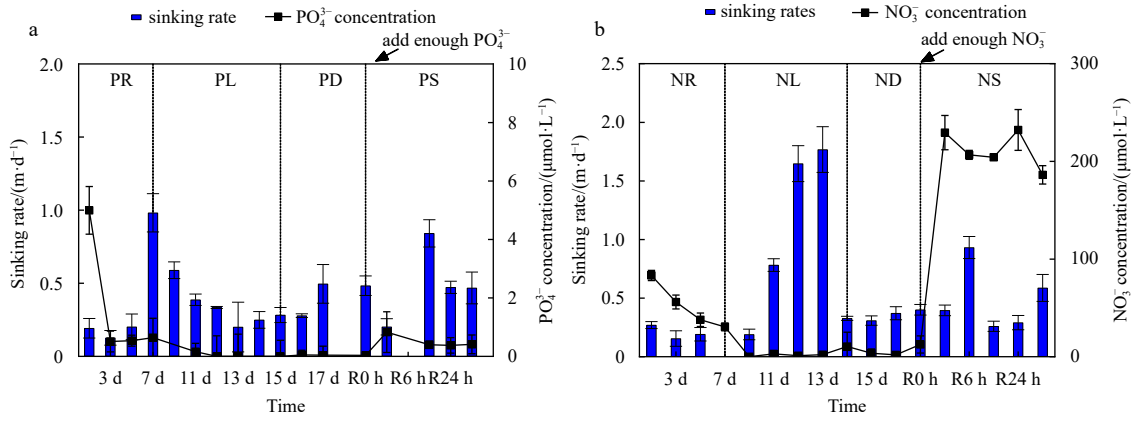

Fig. 3. Limited nutrient concentrations and sinking velocity data for the phosphate depletion-spike experiment (a) and nitrate depletion-spike experiment (b).

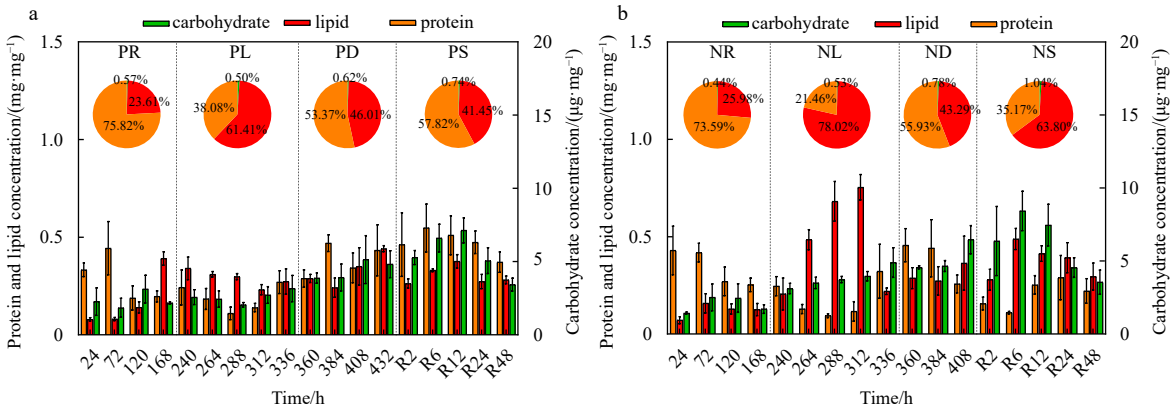

Fig. 4. Intracellular contents (protein, glucose-based carbohydrate, and lipid) data for the phosphate depletion-spike experiment (a) and nitrate depletion-spike experiment (b). The pie chart shows the proportion of each component in four different stages.

T. weissflogii to the two nutrient limitations and spike are discussed below, respectively.

3.1 *Phosphate depletion and spike experiments*

During the first 3 d of the experiment, *T. weissflogii* grew in a logarithmic phase because of PR, with an average growth rate of (0.55 ± 0.08) d^{-1} (Fig. 1a). *Thalassiosira weissflogii* settled at a lower rate during the PR phase, with a mean settling rate of (0.17 ± 0.08) m/d (Fig. 3a) and F_v/F_m of (0.69 ± 0.01) (Fig. 2a). The Chl *a*, protein, carbohydrate, lipid, biosilica, and TEP concentrations were (296.49 ± 27.50) μg/L, (0.32 ± 0.06) mg/mg, (2.42 ± 0.65) μg/mg, (0.10 ± 0.02) mg/mg, (18.90 ± 1.13) μmol/L, and (184.45 ± 62.54) μg/L (Xeq), respectively.

After 7 d of the experiment, extracellular phosphate was gradually depleted and the growth rate decreased to less than 0.3 d^{-1}, indicating the algae cells' PL. The SV significantly increased from (0.20 ± 0.09) m/d to (0.98 ± 0.13) m/d ($P < 0.05$). Throughout the nutrient-limited period 7–15 d, the F_v/F_m values

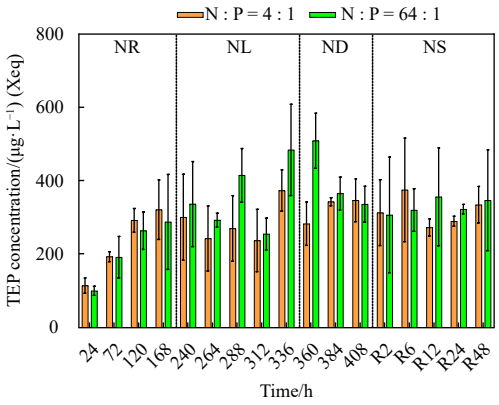

Fig. 5. TEP concentrations in the nitrate depletion-spike experiment (orange pillars) and phosphate depletion-spike experiment (green pillars).

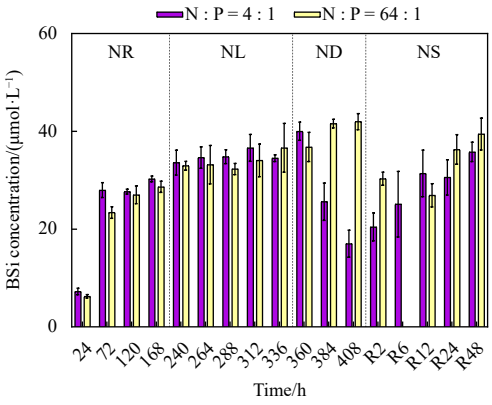

Fig. 6. BSi concentrations in the nitrate depletion-spike experiment (purple pillars) and phosphate depletion-spike experiment (yellow pillars).

Table 1. Changes in F_v/F_m, surface area of a single cell, sinking velocity (SV), and the macromolecular composition, transparent extracellular polymeric particle (TEP) concentrations in *Thalassiosira weissflogii* for the nitrate depletion-spike and phosphate depletion-spike experiments

Nutrient stage	SV/ (m·d^{-1})	Growth rate/d^{-1}	F_v/F_m	Surface area/ μm^2	Protein/ (mg·mg^{-1})	Glucose-based carbohydrate/ (μg·mg^{-1})	Lipid/ (mg·mg^{-1})	TEP/ (μg·L^{-1}) (Xeq)
NR	0.21 ± 0.05	0.55 ± 0.03	0.69 ± 0.01	61.45 ± 14.46	0.34 ± 0.06	2.03 ± 0.52	0.12 ± 0.04	229.38 ± 53.11
NL	1.09 ± 0.13	0.10 ± 0.02	0.59 ± 0.03	73.43 ± 21.17	0.15 ± 0.03	3.58 ± 0.31	0.53 ± 0.07	261.96 ± 87.91
ND	0.35 ± 0.04	0.02 ± 0.05	0.34 ± 0.03	68.17 ± 23.01	0.37 ± 0.10	5.15 ± 0.61	0.28 ± 0.07	336.00 ± 46.30
NS	0.49 ± 0.07	0.04 ± 0.05	0.39 ± 0.02	83.01 ± 20.37	0.20 ± 0.05	6.07 ± 1.33	0.37 ± 0.05	316.50 ± 63.68
PR	0.17 ± 0.08	0.48 ± 0.06	0.69 ± 0.01	81.34 ± 19.04	0.32 ± 0.06	2.41 ± 0.65	0.10 ± 0.02	184.44 ± 62.55
PL	0.45 ± 0.06	0.12 ± 0.04	0.63 ± 0.01	77.77 ± 21.65	0.19 ± 0.05	2.52 ± 0.50	0.31 ± 0.03	344.78 ± 75.24
PD	0.35 ± 0.07	0.06 ± 0.08	0.42 ± 0.02	74.34 ± 24.13	0.38 ± 0.07	4.44 ± 1.25	0.33 ± 0.05	349.88 ± 48.56
PS	0.41 ± 0.07	0.10 ± 0.07	0.40 ± 0.02	95.59 ± 21.54	0.43 ± 0.09	5.55 ± 0.67	0.31 ± 0.03	313.59 ± 110.49

decreased, indicating a decreasing photosynthetic capacity. Compared with the PR phase, carbohydrates insignificantly changed, the protein concentration significantly decreased, the lipid content significantly increased from (0.10 ± 0.02) mg/mg to (0.31 ± 0.03) mg/mg, and the biogenic silica content increased from (18.90 ± 1.13) μmol/L to (32.97 ± 2.88) μmol/L in the PL phase. In contrast, the TEP concentration increased from (184.45 ± 62.54) μg/L (Xeq) to (344.78 ± 75.24) μg/L (Xeq). In the PD phase, the growth rate increased from –0.01 d^{-1} to 0.10 d^{-1} after 8 d of PL (Fig. 3a), which may be attributed to the limiting nutrients being re-released via cell fragmentation. The photosynthetic capacity, SV, and cellular inclusion concentration were significantly decreased, and the lipid content was slightly decreased; however, the carbohydrate content significantly increased from (2.42 ± 0.65) μg/mg to (4.44 ± 1.24) μg/mg, the protein content increased from (0.19 ± 0.05) mg/mg to (0.38 ± 0.07) mg/mg, and TEP and biogenic silica concentrations remained relatively constant.

Under PD conditions, the growth rate and F_v/F_m increased significantly within 12 h after the spike from phosphate addition (456–468 h). The sedimentation rate and lipid content increased from (0.20 ± 0.05) m/d and (0.26 ± 0.02) mg/mg to (0.84 ± 0.09) m/d and (0.38 ± 0.03) mg/mg, respectively. In addition, the protein and TEP concentrations slightly increased during this period. Between 12 h and 48 h after PS treatment, *T. weissflogii* still maintained normal growth and a high photosynthetic capacity, with a gradual increase in the growth rate and F_v/F_m values and a decrease in the SV and lipid content from (0.84 ± 0.09) m/d and (0.38 ± 0.03) mg/mg to (0.47 ± 0.11) m/d and (0.28 ± 0.02) mg/mg, respectively. The protein, carbohydrate, and TEP concentrations fluctuated during this period.

The surface area of single cells for each of the four nutrient salt stages is shown in Fig. 7. In each stage, 30 cells were observed. Because of PL and PD, the cell aggregation enhanced in the late stage, the number of aggregates (diameter > 30 μm) increased significantly, and the single-cell surface area gradually decreased. Approximately 48 h after the PS, the single-cell surface area gradually returned to that of the PR phase.

The correlation between phosphate limitation and spike experimental parameters is shown in Fig. 8a. The results revealed significant negative correlations between F_v/F_m and carbohydrate content (R^2 = –0.77, P < 0.05) and Chl *a* (R^2 = –0.52, P < 0.001). No significant correlation was observed between the SV and protein content, whereas a positive correlation was obtained for the lipid content (R^2 = 0.69, P < 0.001).

3.2 *Nitrate depletion and spike experiments*

During the NR phase, the growth rate of *T. weissflogii* decreased from 0.61 d^{-1} to 0.34 d^{-1} (Fig. 1b), and the F_v/F_m value also decreased from 0.71 to 0.58 (Fig. 2b), indicating nitrate limitation (NL). During the NL phase, the SV increased from (0.21 ± 0.05) m/d to (1.09 ± 0.13) m/d, and the maximum SV reached (1.77 ± 0.02) m/d, which is twice the maximum SV under PL conditions (Fig. 3b). The protein concentration decreased from (0.34 ± 0.06) mg/mg to (0.15 ± 0.03) mg/mg (Fig. 4b), the TEP concentration slightly increased (Fig. 5), the lipid concentration slightly decreased, and both carbohydrate and biosilica concentrations increased significantly from (3.58 ± 0.31) μg/mg and (23.29 ±

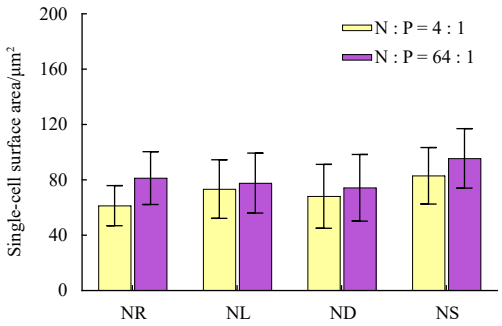

Fig. 7. Single-cell surface area in the four nutrient phases.

1.16) μmol/L to (5.15 ± 0.61) μg/mg and (29.30 ± 2.28) μmol/L, respectively, under NL conditions. After 72 h, the total nitrate concentration and growth rate approached zero, indicating the onset of nitrate depletion (ND). Sinking rates and cellular inclusion concentrations were within the range of measured values for NL.

During the first six hours after the NS, the growth rate of *T. weissflogii* jumped to 0.62 d^{-1}, and then decreased to below 0.3 d^{-1}. The SV increased from (0.40 ± 0.04) m/d to (0.93 ± 0.09) m/d. Biosilica and TEP concentrations also increased. Between 6 h and 24 h after the NS, the photosynthetic capacity of *T. weissflogii* gradually increased, the F_v/F_m value gradually increased from 0.30 to 0.44, and the SV decreased from (0.93 ± 0.09) m/d to (0.29 ± 0.06) m/d. Cellular inclusions, biogenic silica, and TEP concentrations fluctuated during NS.

Figure 8b shows the correlation between parameters in the NL and NS experiments. The results indicate significant negative correlations between F_v/F_m and the carbohydrate content (R^2 = –0.79, P < 0.001) and TEP (R^2 = –0.57, P < 0.001). The SV strongly negatively correlated with the protein content (R^2 = –0.59, P < 0.001) and strongly positively correlated with the lipid content (R^2 = 0.86, P < 0.001).

4 Discussion

4.1 *Response of diatom SV to different nutrient limitations*

The nutrient concentration affects the growth state of the phytoplankton and significantly influences the SV (Smayda and Boleyn, 1965). In most planktonic diatoms, the sinking rate and growth rates are negatively correlated (Eppley et al., 1967; Smayda, 1970; Reynolds and Walsby, 1975). Under conditions with repleted nutrients, the cell growth is vigorous and the algal cells in both sets of experiments grow in a logarithmic phase, with increasing photosynthetic capacity and gradual accumulation of the Chl-*a* content. During this time, the SV of the cells is insignificant. Subsequently, under conditions with limited nutrients, the F_v/F_m, growth rate, and Chl-*a* content produced by a unit of cell decrease and the SV increases sharply. Here, after the nutrient spike, the F_v/F_m continued to increase in the nitrate limitation experiment; however, the cell abundance did not increase significantly, which may be due to the time inconsistency between the photosynthetic response of phytoplankton and its cell abundance growth. Under nitrate limitation, the growth status deteriorates; therefore, it may allocate energy for survival rather than reproduction in the early post-nutrient supplementation period. In addition, the photosystem II of phytoplankton is very responsive to changes in the environment (Kolber et al., 1988). When sinking cells encounter higher concentrations of nutrients, the sinking rate will decrease again (Bienfang et al., 1982). Figure 9 simulates the theoretical relationship between the nutrient limitation and the SV of *T. weissflogii* in the waters of the Changjiang River Estuary as an example.

The SV values of diatoms correlate with the type of limiting nutrient. Bienfang et al. (1982) reported that *Skeletonema costatum*, *Chaetoceros gracilis* and *Ditylum brightwelii* have high SV values under silica-limiting conditions and reduced SV under both NL and PL conditions. *Coscinodiscus wailesii* has high SV values in all three nutrient-limited states (Du Clos et al., 2021). During the nutrient-limited phase of this study, the SV of *T. weissflogii* is significantly higher than that during the nutrient-repleted phase, with a three-fold higher rate in the PL state and an approximately five-fold higher rate in the NL state. The SV was still significantly higher than that during the NR phase, although it decreased during the ND phase. The SV of *T. weissflogii* significantly increased within 6 h of addition of the limited nutrient, gradually returned to the level of the NR stage, and then significantly increased after 24 h, suggesting that the cells may have reentered the NL state. This phenomenon has been observed in studies on *Coscinodiscus wailesii* and *Phaeodactylum tricornu-*

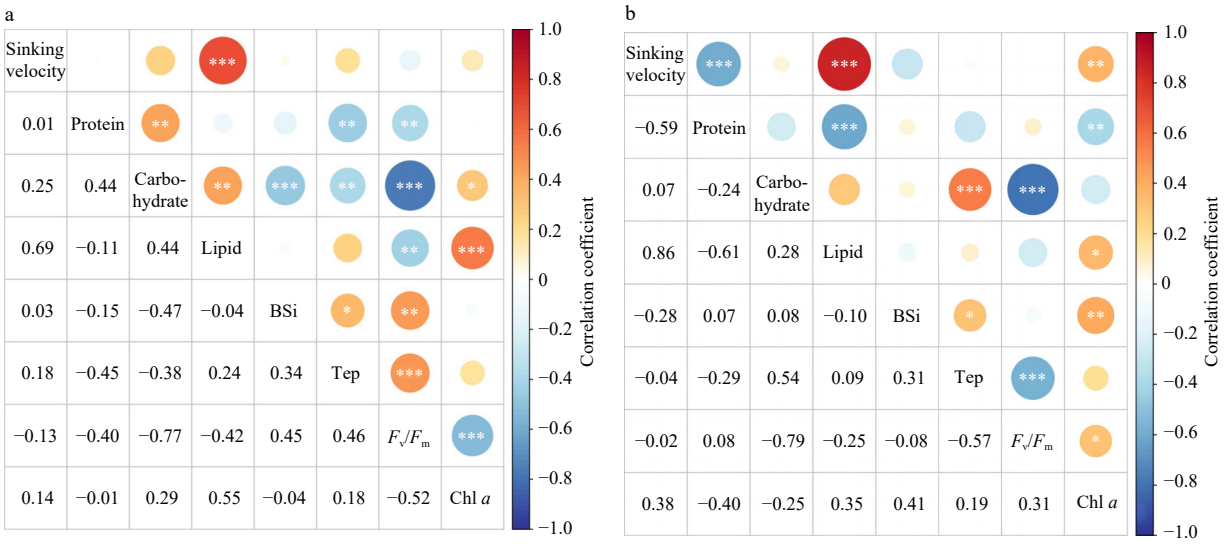

Fig. 8. Correlation between SV and physiological-biochemical parameters for the phosphate depletion-spike experiment (a) and nitrate depletion-spike experiment (b). *: P < 0.05; **: P < 0.01; ***: P < 0.001.

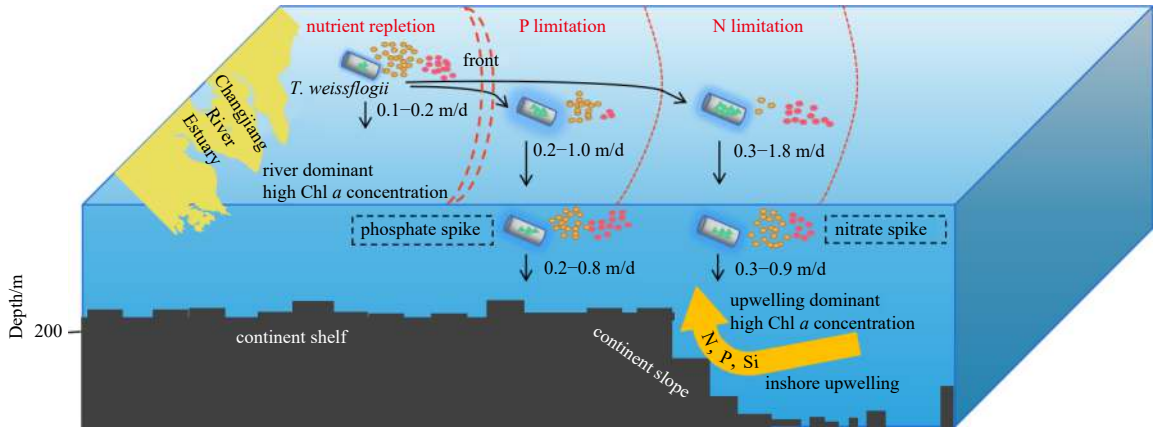

Fig. 9. Conceptual model to simulate the effect of nutrient limitation on the sinking velocity of *Thalassiosira weissflogii* in the Changjiang River Estuary. Owing to the input of diluted water from the Changjiang River, there is an excess of nitrogen and phosphorus nutrient salts. The nearshore waters of the Changjiang River Estuary are in the stage of nutrient repletion without nutrient limitation; however, with the increase in the spreading distance of the freshwater from the Changjiang River, nutrient concentration gradually decreases, and the phenomena of phosphate limitation and nitrate limitation occur successively. Small yellow circles represent nitrate concentrations, red circles represent phosphate concentrations, green triangles represent lipid content and blue shades represent extracellular products.

tum (Du Clos et al., 2021; Zhang et al., 2023). In case of a sudden increase in ambient nutrient concentration, *T. weissflogii* may sink more rapidly, thereby increasing nutrient fluxes. After the internal nutrient reserves of the cell are sufficient, it may slow down its SV, maximizing exposure to light and avoiding the additional energy expenditure associated with sinking.

4.2 *Correlation between cell products and SV*

Under nutrient-limited conditions, *T. weissflogii* may have the capacity to change its cell density by regulating changes in cellular inclusions, thereby controlling the SV. Based on the Stokes equation, the SV of spherical cells will depend on their size and density. Larger and heavier cells may sink at a faster rate. We performed *t*-tests on cell surface area data for both sets of experiments and did not observe significant differences. Therefore, we focused on examining the correlation between cell contents, which are closely related to the density, and their SV values (as shown in Fig. 8). Notably, we observed that the SV values of *T. weissflogii* exhibit significant positive correlations with the lipid content ($P < 0.001$), with an R^2 value of 0.69 in the phosphate limitation experiment and an R^2 value of 0.86 in the nitrate limitation experiment. This result contrasts the conclusions of experimental studies by Smayda (1970) and Pantorno et al. (2013) who suggested that lipid accumulation is not a pivotal mechanism for suspension in phytoplankton and has a limited influence on cell density. Based on other literature, the cell density of diatoms may increase by increasing the intracellular lipid content or altering its composition, thus promoting sedimentation (Alipanah et al., 2018; Van Mooy et al., 2009). It has also been observed that PL and PD increase the lipid content, primarily triglycerides, in the triangular brown fingerling (Reitan et al., 1994). In this study, we observed that the total lipid content, as a percentage of organic compounds, is significantly higher in *T. weissflogii* when it is nutrient-limited (Fig. 4). The percentage of lipids increases from 23.61% to 61.41% under PL conditions and then decreases to 41.45% after the PS. Similarly, the percentage of lipids increases from 25.98% to 78.02% under NL conditions, which dominates the content of organic compounds. The SV reaches the highest level at this stage. Thus, lipids are the key biochemical components that regulate the settling mechanism of *T. weissflogii*.

In addition, protein and carbohydrate contents do not exhibit a significant correlation relationship during the sedimentation of *T. weissflogii*. Proteins are the main macromolecular reservoir of intracellular nitrate; thus NL of the medium has an important effect on protein synthesis (Zhao et al., 2009). In this study, we only observed a significant negative correlation between the SV and protein content in *T. weissflogii* during the NL and ND phases ($R^2 = -0.67$, $P < 0.001$), whereas no significant correlation was recorded during PL. The protein content increases during the ND phase, probably due to the re-release of limiting nutrients resulting from partial cell death and fragmentation. Furthermore, the phosphate uptake capacity of algae increases during starvation depletion, and protein is a major component of excess nitrate accumulation under PL conditions (Rhee, 1978). Similarly, carbohydrates stored in cells under NL and PL conditions show a gradual accumulation trend, which agrees with the results of previous studies (Beardall et al., 2001; Myklestad and Haug, 1972). No significant correlation was observed between biogenic silica and the SV of diatoms.

In addition to cellular inclusions, it has been shown that TEP produced by phytoplankton can also significantly affect SV values (Alldredge et al., 1993; Passow, 2002; Mari et al., 2017; Guo and Sun, 2020). TEP, an extracellular product produced by phytoplankton in the oceans, consists of acidic carbohydrates with colloidal particulate matter properties, which can dissolve by agglutination of organic matter, bacteria, and phytoplankton to form aggregates (Bar-Zeev et al., 2011; Passow, 2002; Simon et al., 2002). Sinking of large aggregates contributes significantly to vertical carbon fluxes, a key factor driving the downward transport of particulate organic carbon. However, TEP are typically less dense than seawater, and in the absence of other particulate ballast, they prefer to remain in surface waters and can even float upwards (Mari et al., 2017). Therefore, the role of TEP in phytoplankton sedimentation is controversial, especially in the real sea, there may be more complex sinking mechanisms. TEP accumulation was observed in our experiments during PL, NL, PD, and ND, with higher levels in the PL state. Staats et al. (2000) reported similar findings based on a nitrate- and phosphate-deficiency study of *T. weissflogii*. In addition, we observed a significant negative correlation between the TEP concentration and SV

during the NL and ND phases (R^2 = –0.77, P < 0.01).

5 Conclusions

(1) Nutrient-limiting conditions significantly affected the SV of diatoms. In the case of *T. weissflogii*, nitrate-limited (N:P = 4:1) and phosphate-limited (N:P = 64:1) conditions could increase the SV up to five- and three-fold, respectively. Short-term increases in restorative nutrients could also increase the SV.

(2) Under both nitrate- and phosphate-limited conditions, the SV variations were related to cellular contents, especially the lipid content. However, the protein content negatively correlated with the SV only under nitrate limitation, and no correlation was observed under phosphate limitation. The glucose-based carbohydrate and biogenic silica contents did not significantly correlate with the SV.

(3) Both nitrate- and phosphate-limited environments induced *T. weissflogii* to produce TEP, and the TEP concentration was higher under phosphate-limited conditions. However, changes in TEP contents under phosphate limitation did not affect SV, whereas SV decreased with increasing TEP levels under nitrate limitation.

This study revealed the sinking mechanism of a single diatom species under nitrate- and phosphate-limited conditions, using controlled indoor culture experiments. However, the aggregation effect of actual phytoplankton populations in the natural marine environment was not considered. The problem of aggregation in the real ocean is widespread, which cannot be ignored. However, in this experiment, the scientific problem we primarily addressed was based on the change of sinking rate of individual cells, and did not focus on the aggregation problem, which is also the limitation of our experiment. In the future, further indoor culture experiments should be conducted to simulate and explore the settling effect of phytoplankton aggregates to elucidate the settling mechanism of phytoplankton under nutrient-limited conditions.

References

Alipanah L, Winge P, Rohloff J, et al. 2018. Molecular adaptations to phosphorus deprivation and comparison with nitrogen deprivation responses in the diatom *Phaeodactylum tricornutum*. PLoS ONE, 13(2): e0193335, doi: 10.1371/journal.pone.0193335

Alldredge A L, Gotschalk C. 1988. *In situ* settling behavior of marine snow. Limnology and Oceanography, 33(3): 339–351, doi: 10.4319/lo.1988.33.3.0339

Alldredge A L, Passow U, Logan B E. 1993. The abundance and significance of a class of large, transparent organic particles in the ocean. Deep-Sea Research Part I: Oceanographic Research Papers, 40(6): 1131–1140, doi: 10.1016/0967-0637(93)90129-Q

Anderson L W J, Sweeney B M. 1977. Diel changes in sedimentation characteristics of *Ditylum brightwelli*: Changes in cellular lipid and effects of respiratory inhibitors and ion-transport modifiers. Limnology and Oceanography, 22(3): 539–552, doi: 10.4319/lo.1977.22.3.0539

Anderson L W J, Sweeney B M. 1978. Role of inorganic ions in controlling sedimentation rate of a marine centric diatom *ditylum brightwelli*. Journal of Phycology, 14(2): 204–214, doi: 10.1111/j.1529-8817.1978.tb02450.x

Bach L T, Boxhammer T, Larsen A, et al. 2016. Influence of plankton community structure on the sinking velocity of marine aggregates. Global Biogeochemical Cycles, 30(8): 1145–1165, doi: 10.1002/2016GB005372

Bar-Zeev E, Berman T, Rahav E, et al. 2011. Transparent exopolymer particle (TEP) dynamics in the eastern Mediterranean Sea. Marine Ecology Progress Series, 431: 107–118, doi: 10.3354/meps09110

Beardall J, Young E, Roberts S. 2001. Approaches for determining phytoplankton nutrient limitation. Aquatic Sciences, 63(1): 44–69, doi: 10.1007/PL00001344

Bienfang P K, Harrison P J, Quarmby L M. 1982. Sinking rate response to depletion of nitrate, phosphate and silicate in four marine diatoms. Marine Biology, 67(3): 295–302, doi: 10.1007/BF00397670

Bienfang P K, Szyper J P. 1982. Effects of temperature and salinity on sinking rates of the centric diatom *Ditylum brightwelli*. Biological Oceanography, 1(3): 211–223

Botte P, d'Ippolito G, Gallo C, et al. 2018. Combined exploitation of CO_2 and nutrient replenishment for increasing biomass and lipid productivity of the marine diatoms *Thalassiosira weissflogii* and *Cyclotella cryptica*. Journal of Applied Phycology, 30(1): 243–251, doi: 10.1007/s10811-017-1221-4

Boyd C, Gradmann D. 2002. Impact of osmolytes on buoyancy of marine phytoplankton. Marine Biology, 141(4): 605–618, doi: 10.1007/s00227-002-0872-z

Bradford M M. 1976. A rapid and sensitive method for the quantitation of microgram quantities of protein utilizing the principle of protein-dye binding. Analytical Biochemistry, 72(1–2): 248–254, doi: 10.1016/0003-2697(76)90527-3

Caspers H. 1970. J. D. H. Strickland and T. R. Parsons: A Practical Handbook of Seawater Analysis. Ottawa: Fisheries Research Board of Canada, Bulletin 167, 1968. 293 pp. $ 7.50. Internationale Revue der gesamten Hydrobiologie und Hydrographie, 55(1): 167

Chen Yaxin, Liu Ruimin, Sun Chengchun, et al. 2012. Spatial and temporal variations in nitrogen and phosphorous nutrients in the Yangtze River Estuary. Marine Pollution Bulletin, 64(10): 2083–2089, doi: 10.1016/j.marpolbul.2012.07.020

Cloern J E. 2001. Our evolving conceptual model of the coastal eutrophication problem. Marine Ecology Progress Series, 210: 223–253, doi: 10.3354/meps210223

Conley D J, Björck S, Bonsdorff E, et al. 2009. Hypoxia-related processes in the Baltic Sea. Environmental Science & Technology, 43(10): 3412–3420

d'Ippolito G, Sardo A, Paris D, et al. 2015. Potential of lipid metabolism in marine diatoms for biofuel production. Biotechnology for Biofuels, 8(1): 28, doi: 10.1186/s13068-015-0212-4

Du Clos K T, Karp-Boss L, Gemmell B J. 2021. Diatoms rapidly alter sinking behavior in response to changing nutrient concentrations. Limnology and Oceanography, 66(3): 892–900, doi: 10.1002/lno.11649

Durante G, Basset A, Stanca E, et al. 2019. Allometric scaling and morphological variation in sinking rate of phytoplankton. Journal of Phycology, 55(6): 1386–1393, doi: 10.1111/jpy.12916

Eppley R W, Holmes R W, Strickland J D H. 1967. Sinking rates of marine phytoplankton measured with a fluorometer. Journal of Experimental Marine Biology and Ecology, 1(2): 191–208, doi: 10.1016/0022-0981(67)90014-7

Granata T C. 1991. Diel periodicity in growth and sinking rates of the centric diatom *Coscinodiscus concinnus*. Limnology and Oceanography, 36(1): 132–139, doi: 10.4319/lo.1991.36.1.0132

Guillard R R, Ryther J H. 1962. Studies of marine planktonic diatoms. I. Cyclotella nana Hustedt, and Detonula confervacea (cleve) Gran. Canadian Journal of Microbiology, 8: 229–239, doi: 10.1139/m62-029

Guo Shujin, Sun Jun. 2020. Concentrations and sinking rates of transparent exopolymer particles (TEPs) in a coastal sea: The Changjiang River (Yangtze River) Estuary. Acta Oceanologica Sinica, 39(10): 58–69, doi: 10.1007/s13131-020-1660-7

Holman W I M. 1943. A new technique for the determination of phosphorus by the molybdenum blue method. Biochemical Journal, 37(2): 256–259, doi: 10.1042/bj0370256

Huisman J, Sommeijer B. 2002. Maximal sustainable sinking velocity of phytoplankton. Marine Ecology Progress Series, 244: 39–48, doi: 10.3354/meps244039

Jin X, Gruber N, Dunne J P, et al. 2006. Diagnosing the contribution of phytoplankton functional groups to the production and export of particulate organic carbon, $CaCO_3$, and opal from glob-

al nutrient and alkalinity distributions. Global Biogeochemical Cycles, 20(2): GB2015

Johnson M B, Wen Zhiyou. 2009. Production of biodiesel fuel from the microalga *Schizochytrium limacinum* by direct transesterification of algal biomass. Energy & Fuels, 23(10): 5179–5183

Kolber Z, Zehr J, Falkowski P. 1988. Effects of growth irradiance and nitrogen limitation on photosynthetic energy conversion in photosystem II. Plant Physiology, 88(3): 923–929, doi: 10.1104/pp.88.3.923

Laurentin A, Edwards C A. 2003. A microtiter modification of the anthrone-sulfuric acid colorimetric assay for glucose-based carbohydrates. Analytical Biochemistry, 315(1): 143–145, doi: 10.1016/S0003-2697(02)00704-2

Lavoie M, Raven J A. 2020. How can large-celled diatoms rapidly modulate sinking rates episodically?. Journal of Experimental Botany, 71(12): 3386–3389, doi: 10.1093/jxb/eraa129

Lavoie M, Raven J A, Levasseur M. 2016. Energy cost and putative benefits of cellular mechanisms modulating buoyancy in aflagellate marine phytoplankton. Journal of Phycology, 52(2): 239–251, doi: 10.1111/jpy.12390

Li Daoji, Zhang Jing, Huang Daji, et al. 2002. Oxygen depletion off the Changjiang (Yangtze River) Estuary. Science in China Series D: Earth Sciences, 45(12): 1137–1146, doi: 10.1360/02yd9110

Liu Sumei, Qi Xiaohong, Li Xiaona, et al. 2016. Nutrient dynamics from the Changjiang (Yangtze River) Estuary to the East China Sea. Journal of Marine Systems, 154: 15–27, doi: 10.1016/j.jmarsys.2015.05.010

Luke C L. 1953. Photometric determination of silicon in ferrous, ferromagnetic, nickel, and copper alloys: A molybdenum blue method. Analytical Chemistry, 25(1): 148–151, doi: 10.1021/ac60073a028

Margalef R. 1978. Life-forms of phytoplankton as survival alternatives in an unstable environment. Oceanologica Acta, 1(4): 493–509

Mari X, Passow U, Migon C, et al. 2017. Transparent exopolymer particles: Effects on carbon cycling in the ocean. Progress in Oceanography, 151: 13–37, doi: 10.1016/j.pocean.2016.11.002

Myklestad S, Haug A. 1972. Production of carbohydrates by the marine diatom *Chaetoceros affinis* var. *willei* (Gran) Hustedt. I. Effect of the concentration of nutrients in the culture medium. Journal of Experimental Marine Biology and Ecology, 9(2): 125–136, doi: 10.1016/0022-0981(72)90041-X

O'Brien K R, Waite A M, Alexander B L, et al. 2006. Particle tracking in a salinity gradient: a method for measuring sinking rate of individual phytoplankton in the laboratory. Limnology and Oceanography: Methods, 4(9): 329–335, doi: 10.4319/lom.2006.4.329

Osibanjo O, Ajayi S O. 1980. Rapid and sensitive spectrophotobetric method for the determination of nitrate in rain water using 3, 4-xylenol. Analyst, 105(1254): 908–912, doi: 10.1039/an9800500908

Pantorno A, Holland D P, Stojkovic S, et al. 2013. Impacts of nitrogen limitation on the sinking rate of the coccolithophorid *Emiliania huxleyi* (Prymnesiophyceae). Phycologia, 52(3): 288–294, doi: 10.2216/12-064.1

Passow U. 2002. Transparent exopolymer particles (TEP) in aquatic environments. Progress in Oceanography, 55(3–4): 287–333, doi: 10.1016/S0079-6611(02)00138-6

Passow U, Alldredge A L. 1995. A dye-binding assay for the spectrophotometric measurement of transparent exopolymer particles (TEP). Limnology and Oceanography, 40(7): 1326–1335, doi: 10.4319/lo.1995.40.7.1326

Ptacnik R, Diehl S, Berger S. 2003. Performance of sinking and non-sinking phytoplankton taxa in a gradient of mixing depths. Limnology and Oceanography, 48(5): 1903–1912, doi: 10.4319/lo.2003.48.5.1903

Raven J A, Doblin M A. 2014. Active water transport in unicellular algae: where, why, and how. Journal of Experimental Botany, 65(22): 6279–6292, doi: 10.1093/jxb/eru360

Reitan K I, Rainuzzo J R, Olsen Y. 1994. Effect of nutrient limitation on fatty acid and lipid content of marine microalgae. Journal of Phycology, 30(6): 972–979, doi: 10.1111/j.0022-3646.1994.00972.x

Reynolds C S, Walsby A E. 1975. Water-blooms. Biological Reviews, 50(4): 437–481, doi: 10.1111/j.1469-185X.1975.tb01060.x

Rhee G Y. 1978. Effects of N: P atomic ratios and nitrate limitation on algal growth, cell composition, and nitrate uptake. Limnology and Oceanography, 23(1): 10–25, doi: 10.4319/lo.1978.23.1.0010

Simon M, Grossart H P, Schweitzer B, et al. 2002. Microbial ecology of organic aggregates in aquatic ecosystems. Aquatic Microbial Ecology, 28(2): 175–211

Smayda T J. 1970. The suspension and sinking of phytoplankton in the sea. Oceanography & Marine Biology, 8: 353–414

Smayda T J, Boleyn B J. 1965. Experimental observations on the flotation of marine diatoms. I. *Thalassiosira cf. nana, Thalassiosira rotula* and *Nitzschia seriata*. Limnology and Oceanography, 10(4): 499–509, doi: 10.4319/lo.1965.10.4.0499

Staats N, Stal L J, Mur L R. 2000. Exopolysaccharide production by the epipelic diatom *Cylindrotheca closterium*: effects of nutrient conditions. Journal of Experimental Marine Biology and Ecology, 249(1): 13–27, doi: 10.1016/S0022-0981(00)00166-0

Tang Danling, Di Baoping, Wei Guifeng, et al. 2006. Spatial, seasonal and species variations of harmful algal blooms in the South Yellow Sea and East China Sea. Hydrobiologia, 568(1): 245–253, doi: 10.1007/s10750-006-0108-1

Tinevez J Y, Perry N, Schindelin J, et al. 2017. TrackMate: An open and extensible platform for single-particle tracking. Methods, 115: 80–90, doi: 10.1016/j.ymeth.2016.09.016

Titman D, Kilham P. 1976. Sinking in freshwater phytoplankton: Some ecological implications of cell nutrient status and physical mixing processes. Limnology and Oceanography, 21(3): 409–417, doi: 10.4319/lo.1976.21.3.0409

Tréguer P, Bowler C, Moriceau B, et al. 2018. Influence of diatom diversity on the ocean biological carbon pump. Nature Geoscience, 11(1): 27–37, doi: 10.1038/s41561-017-0028-x

Turner R E, Rabalais N N, Justic D. 2006. Predicting summer hypoxia in the northern Gulf of Mexico: Riverine N, P, and Si loading. Marine Pollution Bulletin, 52(2): 139–148, doi: 10.1016/j.marpolbul.2005.08.012

Van Mooy B A S, Fredricks H F, Pedler B E, et al. 2009. Phytoplankton in the ocean use non-phosphorus lipids in response to phosphorus scarcity. Nature, 458(7234): 69–72, doi: 10.1038/nature07659

Waite A, Harrison P J. 1992. Role of sinking and ascent during sexual reproduction in the marine diatom *Ditylum brightwellii*. Marine Ecology Progress Series, 87(1): 113–122

Wang Bin, Chen Jianfang, Jin Haiyan, et al. 2017. Diatom bloom-derived bottom water hypoxia off the Changjiang Estuary, with and without typhoon influence. Limnology and Oceanography, 62(4): 1552–1569, doi: 10.1002/lno.10517

Wang Yan, Liu Yongjian, Guo Hao, et al. 2022. Long-term nutrient variation trends and their potential impact on phytoplankton in the southern Yellow Sea, China. Acta Oceanologica Sinica, 41(6): 54–67, doi: 10.1007/s13131-022-2031-3

Wang Baodong, Wang Xiulin, Zhan Run. 2003. Nutrient conditions in the Yellow Sea and the East China Sea. Estuarine, Coastal and Shelf Science, 58(1): 127–136

Yu Rencheng, Lü Songhui, Liang Yubo. 2018. Harmful algal blooms in the coastal waters of China. In: Glibert P M, Berdalet E, Burford M A, et al., eds. Global Ecology and Oceanography of Harmful Algal Blooms. Cham: Springer, 309–316

Zhang Wei, Hao Qiang, Zhu Jie, et al. 2023. Nanoplanktonic diatom rapidly alters sinking velocity via regulating lipid content and composition in response to changing nutrient concentrations. Frontiers in Marine Science, 10: 1255915, doi: 10.3389/fmars.2023.1255915

Zhao Yanfang, Yu Zhiming, Song Xiuxian, et al. 2009. Biochemical compositions of two dominant bloom-forming species isolated from the Yangtze River Estuary in response to different nutrient conditions. Journal of Experimental Marine Biology and Ecology, 368(1): 30–36, doi: 10.1016/j.jembe.2008.09.023

Zhou Feng, Chai Fei, Huang Daji, et al. 2020. Coupling and decoup-

ling of high biomass phytoplankton production and hypoxia in a highly dynamic coastal system: the Changjiang (Yangtze River) Estuary. Frontiers in Marine Science, 7: 259, doi: 10.3389/fmars.2020.00259

Zhou Mingjiang, Shen Zhiliang, Yu Rencheng. 2008. Responses of a coastal phytoplankton community to increased nutrient input from the Changjiang (Yangtze) River. Continental Shelf Research, 28(12): 1483–1489, doi: 10.1016/j.csr.2007.02.009